ELSEVIER

Journal of Non-Crystalline Solids 272 (2000) 179–190

JOURNAL OF NON-CRYSTALLINE SOLIDS

www.elsevier.com/locate/jnoncrysol

Structural and magnetic properties of sodium iron germanate glasses

A. Mekki [a], D. Holland [b,*], Kh.A. Ziq [a], C.F. McConville [b]

[a] *Department of Physics, King Fahd University of Petroleum & Minerals, Dhahran, 31261, Saudi Arabia*
[b] *Department of Physics, University of Warwick, Coventry CV4 7AL, UK*

Received 10 August 1999; received in revised form 23 December 1999

Abstract

A series of sodium iron germanate glasses, with general composition $0.3Na_2O$–xFe_2O_3–$(0.7-x)GeO_2$ ($0 \leqslant x \leqslant 0.15$), has been prepared by conventional melting and casting. The chemical states of the various elemental components have been investigated by X-ray photoelectron spectroscopy (XPS) from fracture surfaces produced in situ. The analysis of the Fe 3p core level spectra of the glasses which contain iron oxide revealed the presence of both Fe^{2+} and Fe^{3+} oxidation states, with the proportion of the Fe^{3+} ions found to increase with increasing Fe_2O_3 content. The O 1s spectra also show composition-dependent changes, with the fraction of non-bridging oxygen atoms also increasing with iron oxide content. Direct current magnetic susceptibility and magnetisation (M) vs magnetic field (H) measurements were also performed on the same samples. The magnetic data support the conclusion that the exchange interaction is antiferromagnetic and increases with increasing Fe_2O_3 content. The fraction of Fe^{2+} ions determined from XPS was found to be in good agreement with values obtained from fitting the M vs H data with a standard Brillouin function.

1. Introduction

It is well established that the structure and properties of glasses containing transition metal ions depend critically on the relative proportions of the different valence states of the particular transition metal. X-ray photoelectron spectroscopy (XPS) has proved to be a powerful technique for investigating the structure of solids, particularly for the identification of valence states and for the study of bridging (BO) and non-bridging oxygen (NBO) in oxide glasses [1]. We have recently used XPS to obtain quantitative information on the NBO content and the transition metal ion oxidation state in several sodium transition metal silicate glasses [2–4]. Iron oxide containing glasses have received particular attention, due to their potential technological applications, and structural studies of these glasses, using a range of techniques, have been briefly reviewed elsewhere [5].

The use of XPS to study the oxidation states of iron in silicate [2], phosphate [6], and borate [7] glasses is well established. It has been found that, in the case of the silicate and phosphate glasses, iron exists in both Fe^{2+} and Fe^{3+} oxidation states and that the concentration of Fe^{3+} increases with

* Corresponding author. Tel.: +44-2476 523 396; fax: +44-2476 692 016.
E-mail address: phsay@csv.warwick.ac.uk (D. Holland).

0022-3093/00/$ - see front matter
PII: S0022-3093(00)00235-0

increasing Fe_2O_3 content. The O 1s photoelectron peaks from the sodium iron silicate glasses could be resolved into two contributions [5], from BO [Si–O–Si] and NBO [Si–O–X], respectively. These relative proportions were found to be consistent with the known glass composition if Fe^{2+} and Fe^{3+} are considered to act as modifier ions. However, the physical properties of these glasses are not consistent with iron oxide behaving as a modifier so, on the premise that iron oxide is in fact an intermediate oxide, it was assumed that oxygen species such as Si–O–Fe and Si–O–Na should be distinguishable. Consequently, O 1s spectra were compared with simulations containing distinct species and an extremely good match was found to the experimental data [2]. It is of interest to assess the validity of such an analysis in the case of sodium iron germanate glasses where there is also the complication of various coordination states of germanium.

The structure of GeO_2 glass has been investigated with a variety of experimental techniques. Recent reports include neutron diffraction [8], high energy photon diffraction (using synchrotron radiation) [9], magic angle spinning nuclear magnetic resonance (MAS NMR) [10] and Raman spectroscopy [11]. The conclusion from these studies is that the structure of vitreous germania resembles that of quartz-like GeO_2, with $[GeO_4]$ tetrahedra providing the basic structural units, giving a continuous random network.

The addition of Na_2O to GeO_2 produces changes in the germanate network which have been interpreted as the formation of 6-fold coordinated germanate polyhedra $[Ge(OGe)_6]^{2-}$, which are charge balanced by Na^+. Alkali germanate glasses exhibit what is referred to as the 'germanate anomaly', where specific physical properties go through either a maximum or a minimum on increasing the alkali metal content of the glass [12–15]. This anomaly relates to the relative populations of 4-fold and 6-fold coordinated Ge, with the latter increasing up to ~20 mol% R_2O (R = Li, Na, K, ...), followed by conversion back to tetrahedral (4-fold) units and NBOs at higher alkali metal concentrations. An alternative model exists, based on the successive formation and destruction of three membered rings, containing only $[GeO_4]$ units [16]. In addition, Weber [17] has used the concept of bond volume to indicate that change in germanium coordination cannot account for the germanate anomaly and has ascribed this to changes in void size. However, EXAFS and X-ray diffraction studies [18–24] show an increase in Ge–O bond length and coordination number up to ~20 mol% Na_2O, followed by a constant value for all higher concentrations. A recent ^{17}O MAS NMR study [25] has also shown that there are no observable NBOs below ~18 mol% Na_2O.

In this paper we have extended our previous work on sodium iron silicate glasses by presenting the first study of the structural and magnetic properties of a series of sodium iron germanate glasses.

2. Experimental

2.1. Sample preparation

The glass samples were prepared using analytical grade powders of Fe_2O_3, Na_2CO_3 (for Na_2O) and GeO_2. Calculated amounts of these powders were mixed and melted in 95% Pt/5% Rh crucibles in the temperature range 1200–1400°C, depending on the Fe_2O_3 concentration, for 2 h. The glass, obtained by fast quenching from the melt, was crushed and then remelted at the same temperature to ensure homogeneity within the overall glass structure. The final melt was then cast into preshaped graphite-coated steel moulds yielding rod specimens with dimensions $6 \times 6 \times 30$ mm^3. After casting, the glasses were transferred to another furnace maintained at 50°C below the glass transition temperature (T_g, having been determined from the differential thermal analysis DTA trace) for 2 h and then cooled to room temperature at a rate of 30°C/h. X-ray powder diffraction analysis indicated that the glasses formed were completely amorphous. After preparation, the samples were stored in a vacuum desiccator prior to insertion in ultra-high vacuum (UHV). Inductively coupled, plasma emission spectroscopy (ICP) showed that the compositions of the glasses were maintained

(±3% of value) within the limits of the accuracy of the technique.

2.2. XPS measurements

The experiments were carried out in a VG Scientific ESCALAB Mk II spectrometer equipped with a dual anode X-ray source (aluminium–magnesium) and a 150 mm concentric hemispherical analyser (CHA). Photoelectron spectra from the C 1s, O 1s, Fe 3p, Na 1s and Ge 3d core levels were recorded, in fixed analyser transmission mode, using a computer controlled data collection system described elsewhere [26]. The XPS measurements were performed using non-monochromatic Al K_α ($h\nu = 1486.6$ eV) radiation from an anode operated at 130 W. The energy scale of the spectrometer was calibrated using the binding energies of Cu $2p_{3/2} = 932.67$ eV, Cu $3p_{3/2} = 74.9$ eV and Au $4f_{7/2} = 83.98$ eV photoelectron lines. The electron energy analyser was operated with a pass energy of 10 eV for the high resolution spectra ($\Delta E \sim 1.0$ eV), whereas a pass energy of 50 eV was used for the routine survey scans.

A glass rod from each composition was fractured in UHV, where the base pressure in the analysis chamber was routinely $<2 \times 10^{-10}$ mbar. The glass bars were notched to guide the fracture, yielding flat uncontaminated surfaces. Fracturing in UHV is considered to be the optimum method of producing a clean surface representative of the bulk composition of the glass. Any other surface treatment (such as ion bombardment) would cause significant changes in the surface composition and chemical state of the glass, especially relating to the alkali metal ion distribution [27]. For consistency, all binding energies are reported with reference to the C 1s transition at 284.6 eV, which arises from minor hydrocarbon contaminants in the vacuum and is generally accepted to be independent of the chemical state of the sample under investigation.

All the spectra presented in this paper have been corrected for shifts associated with any residual charging and the presence of an inelastic background. The O 1s and Fe 3p spectra were fitted with two Gaussian–Lorentzian curves (70% Gaussian) representing NO/BO and NBO, and the possible iron oxidation states, respectively. A non-linear, least-squares algorithm was used to find the best-fit solution in each case. The fraction of NBO was determined from the area ratio of the O 1s spectrum while the Fe^{2+} content was determined from the area ratio of the Fe 3p spectrum. More than one sample was analysed in this manner for each composition and the overall accuracy in the determination of the peak position and chemical shift was ±0.1 eV. The quantitative oxygen bonding (based on relative peak areas) and iron redox analyses were reproducible to ±5% and ±10%, respectively. A period of approximately 2 h was required to collect the necessary data set from each sample and, during this time, no evidence of any X-ray induced reduction of the iron in the glass was observed.

2.3. Magnetic measurements

The magnetisation was recorded, as a function of both magnetic field and temperature (T), using a computer controlled PAR/Lake Shore 4500/150A variable temperature, vibrating sample magnetometer (VSM) incorporating a 9 Tesla superconducting magnet and temperature control in the range 2–300 K. The temperature measuring sensor was a calibrated carbon glass resistor located near the specimen and the VSM was calibrated using a pure nickel standard. The overall accuracy of the temperature measurements was better than ±0.1 K throughout the range, while that of the magnetisation measurements was estimated to be approximately ±5%.

3. Results

3.1. XPS spectra

Relatively low resolution X-ray photoelectron survey scans, in the binding energy region 0–1200 eV, were recorded for each glass sample and are shown in Fig. 1. The core level peaks and X-ray induced Auger lines from the constituent elements are easily identified and marked on the spectra. The small single peak in the binding energy range

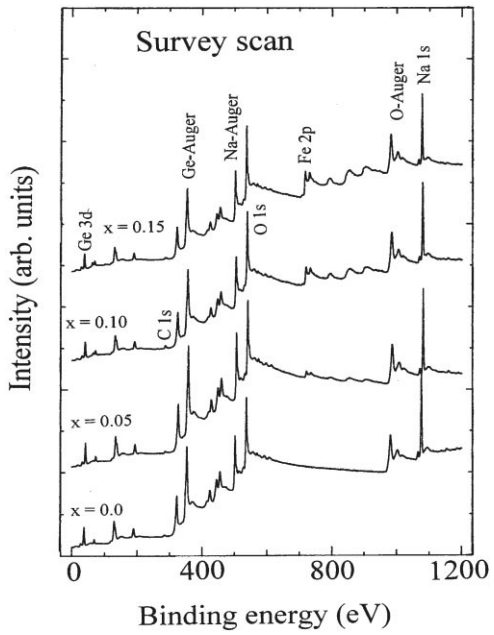

Fig. 1. Survey scan XPS spectra in the energy range 0–1200 eV using Al–K_α X-ray source for the base glass ($x = 0.0$) and the Fe-doped sodium germanate glasses ($x = 0.05$, 0.10 and 0.15).

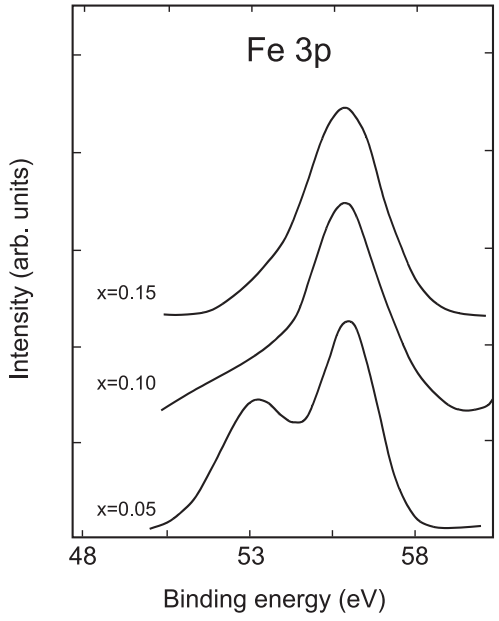

Fig. 2. High resolution core level spectra from the Fe 3p transition for the three Fe-doped glass compositions.

280–300 eV is assigned to the C 1s core level at 284.6 eV.

The doublet in Fig. 1 at ~710 eV arises from Fe 2p photoelectrons and, as expected, this increases in intensity as the Fe_2O_3 content increases. This is the most intense photoelectron peak for iron, however, as has been discussed in our previous work on sodium iron silicate glasses [2], the Fe 2p peaks are broad and occur on a large inelastic background making it impossible to separate and quantify the contributions from the different oxidation states of the Fe ions. In order to quantify the valence state of iron in these germanate glasses, it was necessary to record and analyse the Fe 3p transition in relation to the iron content. Fig. 2 shows higher resolution Fe 3p spectra for the iron oxide containing glasses with various values of x. Two distinct peaks are clearly observed on the spectrum of the lowest Fe content glass ($x = 0.05$) at binding energies of 53.2 eV and 56.0 eV. The lower binding energy peak is seen to decrease with increasing Fe_2O_3 content until becoming a small shoulder for the highest Fe_2O_3 content in the glass ($x = 0.15$). A similar trend is also observed for the Fe 2p spectra (not shown here) and for the Fe doped silicate [2] and phosphate [6] glasses.

The high resolution O 1s photoelectron core level spectra are shown in Fig. 3. The peak at a binding energy of 535 eV is attributed to the Na KLL Auger transition. The intense peak at a binding energy of 530 eV is due to the O 1s transition and seems to be shifting slightly to lower binding energy with increasing iron content in the glass. The peak shape changes with increasing Fe_2O_3 content and the maximum width of the peak (FWHM) is observed for the glass with $x = 0.05$.

Fig. 4 shows the Ge 3d core level peak as a function of composition. The initial binding energy is 31.8 eV, although this shifts to lower binding energy with increasing Fe content reaching 31.0 eV for $x = 0.15$. This shift is significant, as is the associated increase in peak width, and reflects a change in the first coordination sphere of Ge with increasing Fe content in the glass.

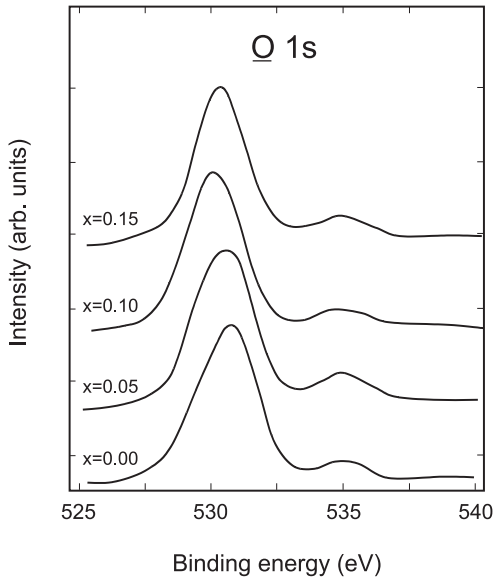

Fig. 3. High resolution core level spectra from O 1s transition for the base glass and the Fe-doped sodium germanate glasses.

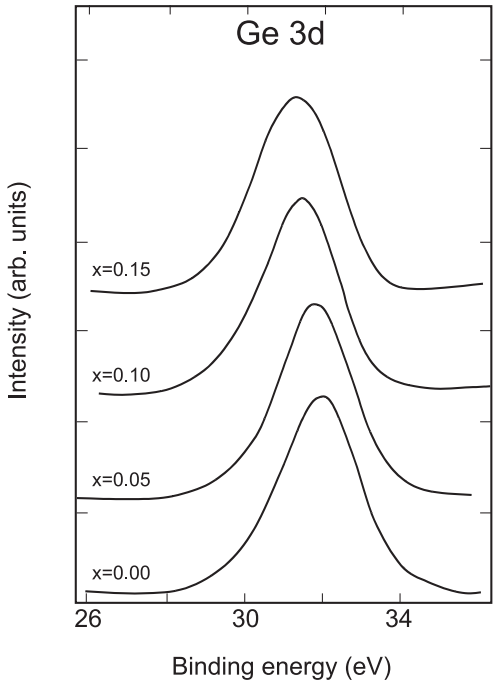

Fig. 4. High resolution core level spectra from Ge 3d transition for the base glass and the Fe-doped glasses.

3.2. Magnetic data

The DC magnetic susceptibility (χ) was calculated by choosing a specific value of applied magnetic field $H(2T)$ and measuring the magnetization (M) in the temperature range 2.5–60 K. The magnetic susceptibility is then simply the ratio M/H. The data in Fig. 5, plotted as χ^{-1} versus T, show that the magnetic susceptibility follows a Curie–Weiss law behaviour, i.e., $\chi = \mathrm{C}(T - \theta_{\mathrm{P}})^{-1}$, where C is the Curie constant and θ_{P} is the Curie temperature. The relevant data obtained from the DC magnetic susceptibility measurements are summarised in Table 1.

The M versus H data measured at different temperatures for the $x = 0.05$ and the $x = 0.15$ glass compositions are shown in Figs. 6(a) and (b), respectively. The magnetisation data at low temperature ($T \leqslant 10$ K) curves toward the field axis. As the temperature is increased, the M versus H curve tends towards linearity, a trend that is observed for all Fe doped glasses. It is also clear from the data that the magnetisation, for the same temperature and field, decreases with increasing Fe_2O_3 content in the glass matrix.

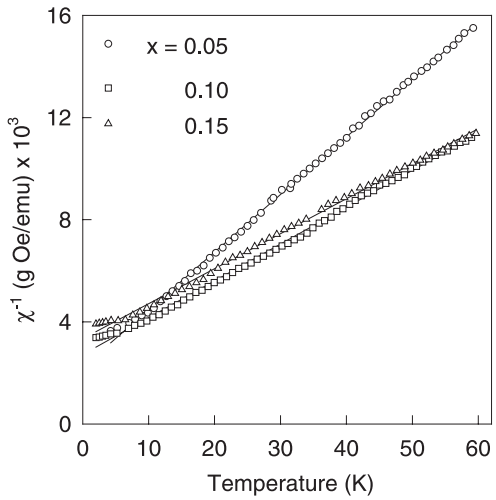

Fig. 5. Inverse DC magnetic susceptibilty (χ^{-1}) in the temperature range 2.5–60 K for the Fe-doped sodium germanate glasses. The solid lines represent the Curie–Weiss law.

Table 1
Parameters derived from the data χ^{-1} versus temperature for the three Fe-doped sodium germanate glasses[a]

x	[Fe ions]/g $\times 10^{20} \pm 0.50 \times 10^{20}$	C (emu K/g) $\times 10^{-3} \pm 0.30 \times 10^{-3}$	$-\theta_P$(°C) $\pm$ 1%	$\mu_{eff}(\mu_B) \pm 0.2$
0.05	6.38	4.55	10.92	5.80
0.10	12.4	6.66	16.65	5.10
0.15	20.9	7.70	28.50	4.80

[a] C is the Curie constant, θ_P is the Curie temperature and μ_{eff} is the effective magnetic moment.

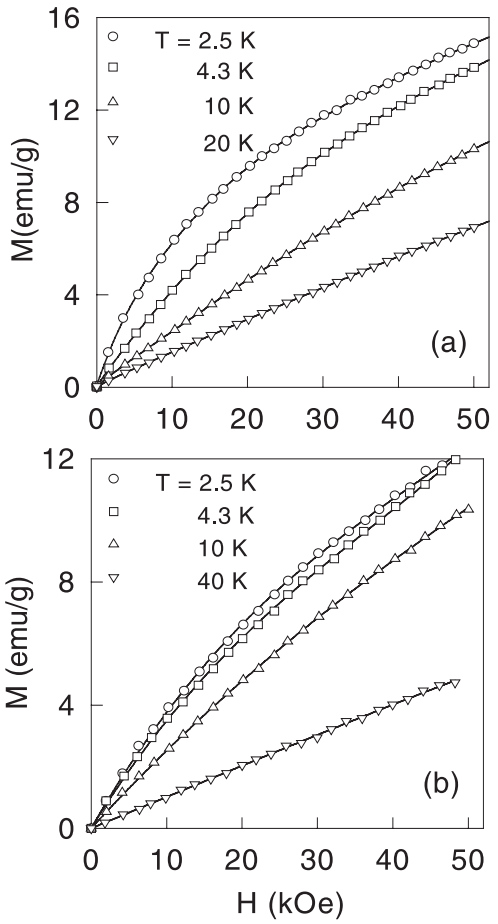

Fig. 6. Magnetization (M) versus magnetic field (H) at different temperatures for (a) $0.05Fe_2O_3$-doped glass, and (b) $0.15Fe_2O_3$-doped glass. The solid lines represent the best fit to the experimental data.

4. Discussion

4.1. XPS results

The binding energy of core level transitions in an XPS spectrum is sensitive to several factors. In the case of transition metal doped glasses, the oxidation state has a significant effect on the binding energy of the transition metal ion. For example, if an element exists in more than one oxidation state, a core level spectrum of that element may well have more than one peak present in the XPS spectrum, each corresponding to a different oxidation state. The shift in the peak position is generally toward the higher binding energy as the oxidation state of the element increases. It is clear from Fig. 2, showing the Fe 3p transition, that there is more than one oxidation state of iron in the Fe doped glasses. Accordingly the peak at binding energy 53.0 eV is assigned to the Fe^{2+} transition and the contribution to the core level peak at a binding energy of 56.0 eV is due to Fe^{3+} ions. In order to quantify the valence state of iron in these germanate glasses, it is necessary to resolve each Fe 3p spectrum into two components. Fig. 7 shows the fitting of the Fe 3p high resolution spectra for the $x = 0.05$ and $x = 0.10$ glass compositions. Using the peak area, the relative proportion of transition metal ions in each oxidation state can be determined and these are reported in Table 2. It is clear from Table 2 that the proportion of Fe^{3+} ions increases with increasing Fe_2O_3 content. Similar trends were also found in the case of Fe–silicate [2] and Fe–phosphate [6] glasses. Information concerning the coordination geometry of the Fe ions in these glasses is not within the resolution capability of our instrument, however, we might expect that the Fe^{3+} at least would be 4-coordinate, as found in the corresponding sodium iron silicates [5].

The XPS spectra obtained by Smets and Lommen for sodium germanate glasses [28] revealed that the O 1s spectrum could be fitted with two peaks, one from BO due to contributions from oxygen atoms in the Ge–O–Ge configuration, and the other from NBO due to contributions from

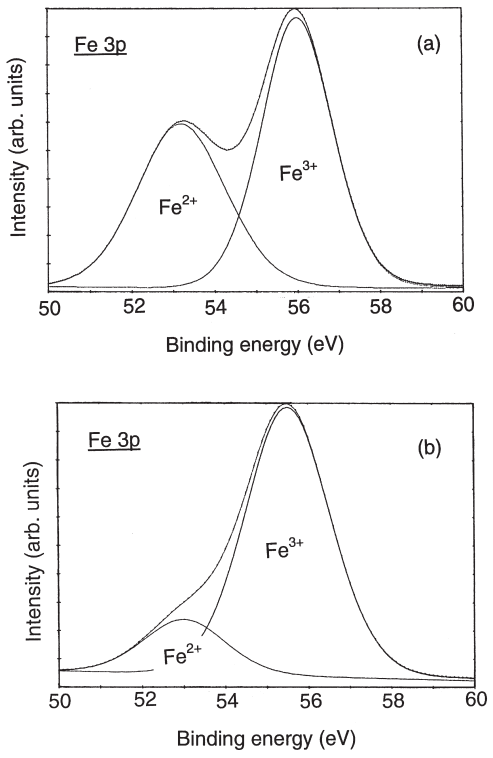

Fig. 7. High resolution Fe 3p core level spectra fitted with Fe^{2+} and Fe^{3+} contributions for (a) $0.05Fe_2O_3$-doped glass, and (b) $0.10Fe_2O_3$ doped glass.

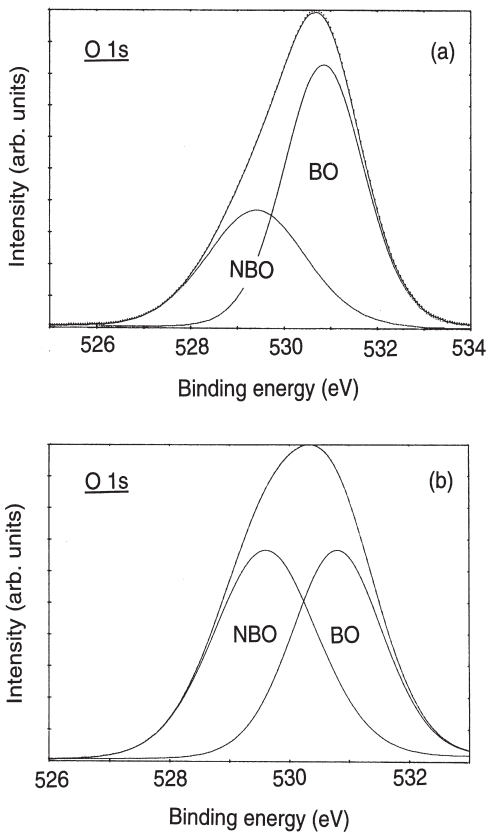

Fig. 8. High resolution O 1s core level spectra fitted with BO and NBO contributions for (a) base glass, and (b) $0.05Fe_2O_3$-doped glass.

oxygen atoms in the Ge–O–Na configuration. The energy separation between the BO and the NBO contributions in alkali germanate glasses was found to be smaller than that in the alkali silicate glasses – values in $0.3Na_2O$–$0.70SiO_2$ and $0.3Na_2O$–$0.70GeO_2$ were found to be 2.1 and 1.6 eV, respectively [28]. The smaller value found in the case of the alkali germanate glass is due to the lower electronegativity of germanium in comparison with silicon.

The high resolution O 1s spectra from the Fe doped sodium germanate glasses are shown in Fig. 3. A fitting procedure, similar to that used to fit the Fe 3p spectra, was applied to each O 1s spectrum and the results are shown in Fig. 8. Two contributions, one due to BO (Ge–O–Ge) and the second due to NBO (Ge–O–Na and Ge–O–Fe), are clearly shown in Figs. 8(a) and (b) for the base

Table 2
Parameters derived from the Fe 3p core level spectra of the Fe-doped sodium germanate glasses[a]

x	Binding energy (eV)		FWHM (eV)		$\Delta E_{Fe2+-Fe3+}$ (eV)	$[Fe^{2+}]/Fe_{total}$ (%)
	Fe^{2+}	Fe^{3+}	Fe^{2+}	Fe^{3+}		
0.05	53.0	56.0	2.6	2.5	3.0	43
0.10	53.0	55.5	2.4	2.5	2.5	16
0.15	52.8	55.4	2.4	2.5	2.6	7

[a] The experimental error in the energy measurements is estimated to be ±0.2 eV. The error in the redox state measurements is ±10%.

glass and $x = 0.05$ glass composition, respectively. It was not possible to resolve the individual contributions from Ge–O–Fe^{2+}, Ge–O–Fe^{3+}, and Ge–O–Na^{+} as the binding energy separations between these contributions to the O 1s are too small. The NBO to total oxygen (TO) ratios obtained from the fit of the O 1s spectra are reported in Table 3 for all of the glass samples. The values show that the proportion of NBO increases with increasing Fe_2O_3 content. In the case of the base glass, the energy separation of the BO and the NBO peaks is 1.6 eV and the ratio NBO/TO is 35%, both deduced from the fit of the O 1s spectrum. These values are in good agreement with the previous work of Smets and Lommen [28]. The increase in NBO concentration with increasing Fe_2O_3 content in the glass suggests that both Fe^{2+} and Fe^{3+} ions behave as network modifiers. Based on this assumption, the ratio of NBO to TO calculated from the glass composition would be given as

$$\frac{[\mathrm{NBO}]}{[\mathrm{TO}]} = \frac{2[\mathrm{Na_2O}] + 6[\mathrm{Fe_2O_3}] + 4[\mathrm{Fe_2O_2}]}{[\mathrm{Na_2O}] + 2[\mathrm{GeO_2}] + 3[\mathrm{Fe_2O_3}] + 2[\mathrm{Fe_2O_2}]}. \quad (1)$$

The ratio of NBO to TO calculated from Eq. (1) for each glass sample is reported in Table 3. Good agreement is found between the measured and calculated values of the NBO content consistent with both Fe^{2+} and Fe^{3+} entering the glass as network modifying ions.

The Ge 3d transition shows a significant shift to lower binding energy with increasing Fe_2O_3 content in the glass. Since the binding energy of the Ge 3d electrons decreases by 0.7 eV on going from quartz-like GeO_2 (4-coordinated Ge) to rutile-like GeO_2 (6-coordinated Ge) [29], this shift in the glasses could be consistent with an increase in the coordination of Ge with increasing Fe_2O_3. It could also indicate an increasing number of NBOs attached to Ge. Therefore, in the base glass ($x = 0$) and the lowest Fe_2O_3 content ($x = 0.05$) glass, the majority of germanium atoms exist in a [GeO_4] tetrahedral coordination while for $x = 0.10$ and $x = 0.15$, either the average germanium atom coordination is increasing, or the iron species are producing an increase in the average number of NBO per germanium. It should be noted that the successful use of Eq. (1) implies that there is *no* significant quantity of 6-coordinated Ge species in the glasses, since these would effectively eliminate twice their number of NBOs.

The other potential mechanism for eliminating NBOs [$Ge(OGe)_3O^-Na^+$] would be the formation of [$Fe(OGe)_4^-Na^+$] units in which a tetrahedral [FeO_4] unit replaces [GeO_4] but, because of the +3 charge on Fe, the unit carries negative charge which is then compensated by Na^+ without the need for NBOs. At the same time, Ge–O^-Na^+ would be replaced by Ge–O–Fe linkages in which there is significant covalency and directionality in the O–Fe bond. This is analogous to the formation of [$Al(OSi)_4^-Na^+$] units in aluminosilicates.

The glass forming range in this system and the physical properties of these glasses are consistent with Fe–O bonding having more directional character than Na–O and therefore an attempt was made to simulate the O 1s spectra of the iron doped glasses in order to separate the different contributions to the non-bridging oxygen peak which arise from Ge–O–Na, Ge–O–Fe(II) and Ge–O–Fe(III). To do this, the Z/r ratio of the ions bonded to the oxygens was taken as a measure of their ability to remove charge from the oxygen and thus increase the O 1s binding energy (Z being the nominal charge on the ion and r being the mean radius in nm). The Z/r values are Ge^{4+} (74.0), Na^+ (9.8), Fe^{2+} (32.8), and Fe^{3+} (54.5), respectively. These numbers can then be used to derive values for the O 1s binding energy of Ge–O–Fe(II) and Ge–O–Fe(III) contributions by a linear interpolation between the observed values for the Ge–O–Ge

Table 3
The BO–NBO energy separation and the measured proportion of NBO found by fitting the core level O 1s spectra for all the germanate glasses[a]

x	$\Delta E_{\mathrm{BO-NBO}}$ (eV)	[NBO]/[TO] % measured	[NBO]/[TO] % calculated
0.0	1.6	35	35
0.05	1.3	53	48
0.10	1.2	59	61
0.15	1.0	71	74

[a] The accuracy in the measured ratio is ±5%. The calculated proportions of NBO are based on Eq. (1). TO is the total oxygen content in the glass.

and Ge–O$^-$Na$^+$ ($x = 0$). On this simple basis one might expect that, as iron oxide is substituted for GeO_2, the O 1s contributions from the Ge–O–Ge configuration at 531.0 eV would be replaced by peaks for Ge–O–Fe(II) and Ge–O–Fe(III) at positions of approximately 530.0 eV and 530.5 eV respectively. The Ge–O$^-$Na$^+$peak can be considered to remain at 529.4 eV since no change in the Na content has occurred.

Fig. 9 shows the simulation of the O 1s peak based on the above model for the $x = 0.05$ Fe_2O_3 glass composition. This was produced using a Gaussian–Lorentzian function with a Gaussian contribution equal to the experimental value, a half-width based on the value from the base glass ($x = 0$) sample and intensities calculated from the chemical composition and the Fe^{2+}/Fe^{3+} ratios determined from the XPS data. It is clear from Fig. 9 that the proposed model, based on the chemistry and the composition of the glass, successfully reproduces the experimental data for this glass composition. An attempt was also made to fit the higher Fe content glasses; however, it was not possible to obtain a satisfactory fit using the same approach for glasses with $x > 0.05$ Fe_2O_3. This may be because this simple model does not include the possibility of [GeO_6] or the effect of the formation of [$Fe(OGe)_4^-Na^+$] units, both of which could be present. However, a more likely explanation is the fact that simulations of the O 1s spectra in sodium iron germanate glass requires significantly higher resolution data than that obtainable with the instrument used here. Additional evidence, such as confirmation of the coordination of the iron species, provided by Mössbauer spectroscopy, neutron diffraction and EXAFS would also be beneficial.

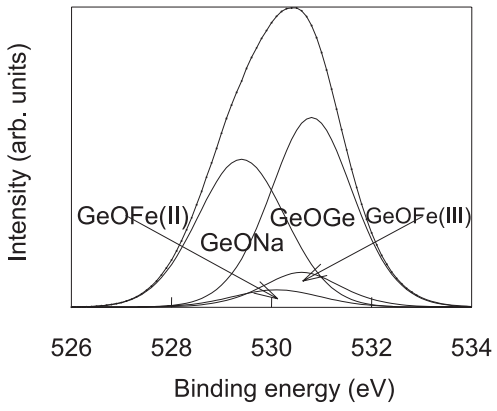

Fig. 9. Comparison of the observed data (dots) with the intensity distribution calculated (solid line) by simulating the contributions from Ge–O–Ge, Ge–O–Na, Ge–O–Fe(II) and Ge–O–Fe(III).

The formation of [$Fe(OGe)_4^-Na^+$] units in sodium iron germanate glasses is analogous to the formation of [$Al(OSi)_4^-Na^+$] units in sodium aluminosilicate glasses. Smets and Lommen have performed XPS studies of such glasses [30] and report a rapid increase in the BO peak, at the expense of the NBO peak, with increasing Al_2O_3. The NBO peak completely disappears when the Al_2O_3 concentration equals the Na_2O concentration. However, their data is plotted as a function of binding energy *shift* from the peak *maximum*, which they associate with the BO. If their data are replotted so that the Na KLL Auger peaks are aligned in all the spectra, it can clearly be seen that the actual effect of substituting Al_2O_3 for SiO_2 is to produce additional intensity at binding energies which lie *between* those of the BO and the NBO peaks. This additional O 1s intensity must be due to photoelectrons emanating from the Si–O–Al species. This behaviour is similar to the changes seen in O 1s spectra from sodium iron silicate glasses [2] and in the sodium iron germanate samples reported here (the Z/r value of Al^{3+} is 56.6, compared with 54.5 for Fe^{3+}). A study using Raman spectroscopy to investigate sodium aluminogermanate glasses with $Na_2O{:}Al_2O_3 = 1{:}1$ indicated the presence of only [AlO_4] and [GeO_4] polyhedra [31].

The [$Al(OSi)_4^-$] unit in aluminosilicate glasses is perceived as possessing some degree of covalency, such that there is a well defined [AlO_4] polyhedral unit, similar to the [SiO_4] tetrahedron. A degree of localisation of the bonding electrons gives some directionality to the bonding and constrains molecular motion in the glass. This leads to lower thermal expansion coefficients and higher values of T_g, compared with sodium silicate glasses containing the same amount of sodium. Since the Z/r values are similar for Al^{3+} and Fe^{3+} it is reasonable to assume that there should be a similar

amount of charge localisation in the O–Fe bond and that the [FeO_4] polyhedron can indeed be regarded as analogous to the [AlO_4] polyhedron, producing similar effects in the physical properties. However, to claim the existence of well-defined [$Fe(OGe)_4^- Na^+$] units is probably not justified by the data presented here.

In each case XPS demonstrates that for all these systems the binding energies of the O 1s electrons in units such as M–O–M′ (where M is a network former such as Si or Ge) decrease as M′ goes from being a network former, to an 'intermediate' and then finally to a modifier. The polyhedral unit formed by the intermediate displays a greater displacement of electronic charge from the cation to the oxygens than is found in the network former polyhedral units. However, there is still sufficient bond directionality to produce physical properties that are significantly different from those of glasses containing modifier polyhedral units where the charge displacement from the cation to the oxygen is almost complete.

4.2. Magnetic data

The negative value for the Curie temperature (Table 1) indicates clearly that the magnetic exchange interaction is antiferromagnetic in all the Fe doped glasses and, as expected, $|-\theta_P|$ increases as more magnetic Fe ions are introduced in the glass and the magnetic ion–ion interaction becomes stronger. The increase in the exchange interaction is confirmed in Fig. 10, in which the magnetisation M is plotted as a function of the reduced variable H/T. A collapse of the magnetic data to a single curve would indicate that the magnetic ion–ion interaction is weak and paramagnetic, as has been seen previously in Cu doped silicate glasses [32] and Gd doped lead borate glasses [33]. However, the failure of the current magnetic data to behave in this manner implies that the exchange interaction is strong, as has been seen in the case of Co doped silicate glasses [4]. The increased divergence of the data sets with increasing x again indicates that the magnetic ion–ion exchange interaction becomes stronger as more Fe_2O_3 is introduced into the glass.

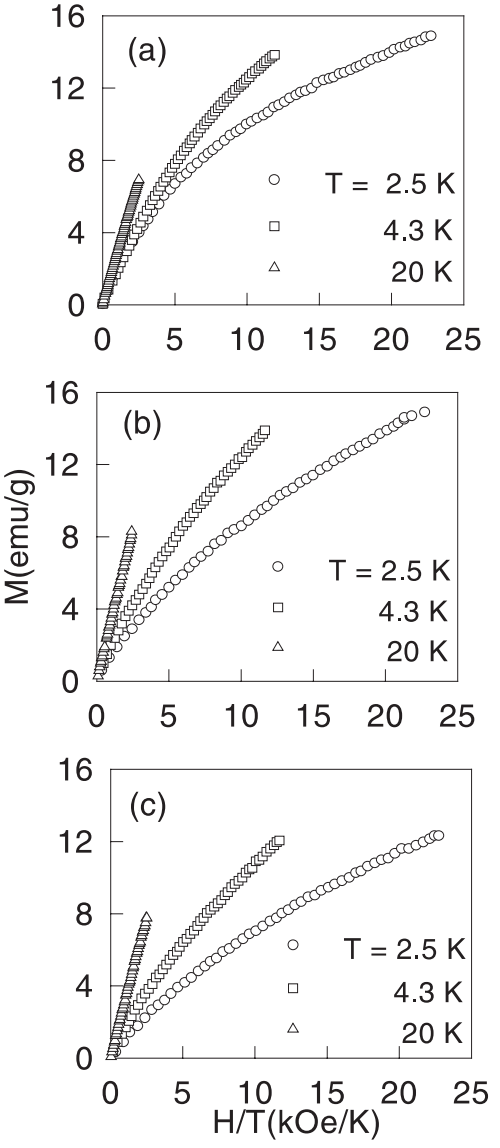

Fig. 10. Magnetization data for the Fe_2O_3-doped glasses taken at three different temperatures and plotted against the reduced variable H/T.

The magnetic data (M versus H) was fitted by the following equation:

$$M = NgJ\mu_B B_J(y), \tag{2}$$

where

$$B_J(y) = \frac{2J+1}{2J}\coth\left[\frac{2J+1}{2J}y\right] - \frac{1}{2J}\coth\left[\frac{y}{2J}\right]$$

Table 4
Concentration of Fe^{2+} ions/g $\times 10^{20}$ and the ratio $[Fe^{2+}]/Fe_{total}$ needed to fit the magnetic data M versus H for three representative temperatures for the Fe-doped sodium germanate glasses

x	2.5 K		4.3 K		10 K	
	$[Fe^{2+}]$	$[Fe^{2+}]/Fe_{total}$ %	$[Fe^{2+}]$	$[Fe^{2+}]/Fe_{total}$ %	$[Fe^{2+}]$	$[Fe^{2+}]/Fe_{total}$ %
0.05	2.54	39.8	2.71	42.5	2.86	44.8
0.10	1.78	14.4	1.88	15.2	1.94	15.6
0.15	1.38	6.59	1.45	6.92	1.42	6.78

is the Brillouin function. M the total magnetisation, N the number of magnetic ions, J the total angular momentum, μ_B the Bohr magneton and g is the Landé splitting factor (equal to 2 for spin-only). The value of y is generally taken to be equal to $gJ\mu_B H/k_B T$ when the magnetic ions behave paramagnetically. However, in this case, the value of y will be modified to $y = gJ\mu_B H/k_B(T-\theta_P)$ to take into account the exchange interaction between the Fe ions in the glass matrix, where θ_P will take the values reported in Table 1 depending on the glass composition.

The magnetisation data for each glass sample were fitted to Eq. (2) with contributions from Fe^{2+} and Fe^{3+} ions, since both ions contribute to the total magnetisation. For Fe^{2+} ion, $J_1 = S_1 + L_1 = 2 + L_1$, while for Fe^{3+} ion, $J_2 = S_2 = 5/2$ since $L_2 = 0$. Transition metal ions in glasses generally show spin-only type moments [34] and it has also been found that the angular momentum of Fe^{2+} ions in silicate glasses is quenched [35]. Furthermore, attempts to fit the experimental data using Eq. (2) with L_1 taking values in the range $0 < L_1 < 2$ resulted in unphysical negative values for the number of Fe^{2+} ions, the fitting parameter. Therefore, the angular momentum of Fe^{2+} ions is also quenched in germanate glasses and L_1 should take the value zero in the calculations. Eq. (2) can be rewritten as

$$M_{total} = M(Fe^{2+}) + M(Fe^{3+}) = N_1 g J_1 \mu_B B_{J_1}(y_1) + (N - N_1) g J_2 \mu_B B_{J_2}(y_2), \quad (3)$$

where $y_1 = gJ_1\mu_B H/k_B(T-\theta_P)$ and $y_2 = gJ_2\mu_B H/k_B(T-\theta_P)$. The number N_1 (number of Fe^{2+} ions/g of the sample) was used as the adjustable parameter to obtain the best fit to the experimental data. The fitting of the experimental data is shown in Figs. 6(a) and (b) for two compositions only. The number of Fe^{2+} ions needed to fit the data at different temperatures is shown in Table 4. The $[Fe^{2+}]/[Fe_{total}]$ ratios obtained from the magnetic measurements and from the XPS measurements are in good agreement for all Fe doped glasses. It should also be noted that while XPS is a surface sensitive technique, the magnetic measurements relate to bulk properties. The agreement between these two techniques is therefore an indication that a fractured sample in ultra high vacuum is the most appropriate surface to be studied as it is clearly the most representative of the bulk state.

5. Conclusions

Information relating to the redox state of iron in a series of sodium germanate glasses has been obtained from XPS. Quantitative analysis of the valence (charge) state of these glasses was found to be in good agreement with values obtained from magnetic measurements performed on the same samples. The O 1s spectra were resolved into BO and NBO contributions. Oxygens in Ge–O–Fe^{2+} and Ge–O–Fe^{3+} sites both contributed to the 'NBO' signal, possibly indicating that both Fe^{2+} and Fe^{3+} behave as network modifiers, but glass-forming ability and physical properties are more typical of intermediate oxides. Attempts to simulate the O 1s with contributions from Ge–O–Ge, Ge–O–Na and Ge–O–Fe species were only successful for $x = 0.05$. It was observed, from the magnetic susceptibility measurements, that the magnetic exchange interaction between Fe ions is antiferromagnetic and its strength increases with increasing Fe_2O_3 content in the glass. This was also

confirmed graphically by the non-collapse of the magnetic data on the M versus H/T representation.

Acknowledgements

Two of the authors (A.M. and Kh.A.Z.) would like to acknowledge the support of King Fahd University of Petroleum and Minerals, Saudi Arabia.

References

[1] C.G. Pantano, in: C.J. Simmons, O.H. El-Bayoumi (Eds.), Experimental Techniques in Glass Science, American Ceramic Society, Westerville, OH, 1993 (Chapter 5).
[2] A. Mekki, D. Holland, C.F. McConville, M. Salim, J. Non-Cryst. Solids 208 (1996) 267.
[3] A. Mekki, D. Holland, C.F. McConville, J. Non-Cryst. Solids 215 (1997) 271.
[4] A. Mekki, D. Holland, Kh.A. Ziq, C.F. McConville, J. Non-Cryst. Solids 220 (1997) 267.
[5] D. Holland, A. Mekki, I.A. Gee, C.F. McConville, J.A. Johnson, C.E. Johnson, P. Appleyard, M. Thomas, J. Non-Cryst. Solids 253 (1999) 192.
[6] R.K. Brow, C.M. Arens, X. Yu, E. Day, Phys. Chem. Glasses 35 (1994) 132.
[7] R. Kamal, S.W. Ali, J. Non-Cryst. Solids 87 (1986) 415.
[8] D.L. Price, M.L. Saboungi, Phys. Rev. Lett. 15 (1998) 3207.
[9] J. Neuefeind, K.D. Liss, Ber. Bunsenges. Phys. Chem. 100 (1996) 1341.
[10] R. Hussin, R. Dupree, D. Holland, J. Non-Cryst. Solids 246 (1999) 159.
[11] D.J. Durban, G.H. Wolf, Phys. Rev. B 43 (1991) 2355.
[12] A.O. Ivanov, K.S. Evstropiev, Dokl. Akad. Nauk. SSSR 145 (1962) 797.
[13] E.F. Riebling, J. Chem. Phys. 39 (1963) 1889.
[14] E.F. Riebling, J. Chem. Phys. 39 (1963) 3022.
[15] M.K. Murthy, J. Ip, Nature 201 (1964) 285.
[16] G.S. Henderson, M.E. Fleet, J. Non-Cryst. Solids 134 (1991) 259.
[17] H.-J. Weber, J. Non-Cryst. Solids 243 (1999) 220.
[18] S. Sakka, K. Kamiya, J. Non-Cryst. Solids 49 (1982) 103.
[19] C. Yin, K. Lu, Y. Zhao, J. Non-Cryst. Solids 112 (1989) 96.
[20] C.D. Yin, H. Morikawa, F. Maruno, Y. Gohshi, Y.Z. Bai, S.J. Fukashima, J. Non-Cryst. Solids 69 (1984) 279.
[21] K. Kamiya, T. Yoko, Y. Itoh, S. Sakka, J. Non-Cryst. Solids 79 (1986) 285.
[22] K. Kamiya, T. Yoko, Y. Miki, Y. Itoh, S. Sakka, J. Non-Cryst. Solids 91 (1987) 279.
[23] K. Kamiya, S. Sakka, Phys. Chem. Glasses 20 (1979) 60.
[24] M. Ueno, M. Misawa, K. Suzuki, Physica B 120 (1983) 347.
[25] R. Hussin, D. Holland, R. Dupree, J Non-Cryst. Solids 232–234 (1998) 440.
[26] A. Mekki, Ph.D. Thesis, University of Warwick, UK, 1997.
[27] B.M.J. Smets, T.P.A. Lommen, J. Am. Ceram. Soc. 65 (1984) 95.
[28] B.M.J. Smets, T.P.A. Lommen, J. Non-Cryst. Solids 46 (1981) 21.
[29] I.A. Gee, D. Holland, R. Hussin, C.F. McConville, A. Mekki, Phys. Chem. Glasses 41 (2000) 203.
[30] B.M.J. Smets, T.P.A. Lommen, Phys. Chem. Glasses 22 (1981) 158.
[31] S.K. Sharma, D.W. Matson, J. Non-Cryst. Solids 69 (1984) 81.
[32] A. Mekki, D. Holland, Kh.A. Ziq, C.F. McConville, Phys. Chem. Glasses 39 (1998) 45.
[33] S.K. Mendiratta, M.A. Valente, J.A. Parenboom, J. Non-Cryst. Solids 134 (1991) 100.
[34] E. Baiocchi, A. Montenero, B. Bettinelli, J. Non-Cryst. Solids 46 (1981) 203.
[35] A. Mekki, Kh.A. Ziq, in: presented at the 22nd International Conference on Low Temperature Physics (LT22), Helsinki, Finland, August 1999.